

## Effects of Chelating Agents on Electrochemical Behavior and Microstructure of Phosphate Conversion Coatings on Magnesium Alloy AZ91D

Yong Zhou<sup>1,2</sup>, Qing yun Xiong<sup>1,2</sup>, Jin ping Xiong<sup>1,2,\*</sup>, Jian yun He<sup>3,\*</sup>

<sup>1</sup> Beijing Key Laboratory of Electrochemical Process and Technology of Materials, Beijing University of Chemical Technology, Beijing 100029, China

<sup>2</sup> Key Laboratory of Carbon Fiber and Functional Polymer of Education Ministry, Beijing University of Chemical Technology, Beijing 100029, China

<sup>3</sup> College of Mechanical and Electrical Engineering, Beijing University of Chemical Technology, Beijing 100029, China

\*E-mail: [xiongjp@mail.buct.edu.cn](mailto:xiongjp@mail.buct.edu.cn); [jyhe2009@163.com](mailto:jyhe2009@163.com)

Received: 24 April 2014 / Accepted: 18 May 2014 / Published: 16 June 2014

---

This paper involved the phosphate conversion coatings formed on the magnesium alloy AZ91D from various phosphating baths, each containing one of the following chelating agents: tetrasodium pyrophosphate (TSPP), amino trimethylene phosphonic acid (ATMP), and ethylene diamine tetraacetic acid (EDTA). The effects of the chelating agents on the electrochemical behavior, microstructure, composition, and corrosion protection of the phosphate conversion coatings were investigated by using potentiodynamic polarization (PDP) curves, electrochemical impedance spectroscopy (EIS) plots, scanning electron microscopy (SEM) observations, X-ray diffraction (XRD) analyses, X-ray photoelectron spectroscopy (XPS) analyses, and salt-water immersion (SWI) tests. The results showed that adding TSPP refined the microstructure of the crystal clusters. The results also showed that the phosphate conversion coating derived from the phosphating bath containing TSPP, with the most uniform, compact, and integral crystal clusters, provided better corrosion protection for the magnesium alloy AZ91D than that derived from the phosphating bath containing ATMP or EDTA. According to XPS results, the phosphate conversion coatings were composed of P, O, Zn, Mg, and Al. XRD showed that the major phases of the coatings were  $Zn_3(PO_4)_2$ ,  $Zn_2Mg(PO_4)_2$ , and Zn.

---

**Keywords:** electrochemical behavior; microstructure; magnesium alloy AZ91D; phosphate conversion coating; chelating agent

### 1. INTRODUCTION

Magnesium alloys have many excellent properties: low density, high thermal conductivity, good electromagnetic features, high strength to weight ratio, and good recyclability. In the aerospace,

automobile, and electronic industries, magnesium alloys are often used for manufacturing components and instruments [1-3]. Unfortunately, the natural oxide layer on the surface of magnesium alloys is very thin and loose and cannot provide good corrosion protection for magnesium alloys [4, 5]. Therefore, the corrosion susceptibility of magnesium alloys is higher than that of other metal alloys and limits the wide applications of magnesium alloys [6, 7]. The common surface treatments to strengthen the corrosion resistance of magnesium alloys include anodizing layers, metal coatings, laser surface treatments, and chemical conversion coatings. Chemical conversion coatings, including chromate conversion coatings and phosphate conversion coatings, have some advantages: easy operation, low cost, and little size limitation. The corrosion protection of chromate conversion coatings for magnesium alloys has been widely investigated, and the hexavalent chromium in chromating baths has been found to be carcinogenic. Therefore, phosphate conversion coatings—the environmentally friendly alternative—are replacing chromate conversion coatings [8, 9]. As a primer on the surface of metals, phosphate conversion coatings have been used for carbon steels and aluminum alloys because these coatings can strengthen the adhesion between organic coatings and basal metals [10-12]. However, it is difficult to prepare phosphate conversion coatings on magnesium alloys because of the chemical and electrochemical activities of magnesium. Recently, phosphate conversion coatings on magnesium alloys have been investigated by many researchers [13-16]. In most investigations, a metal salt such as molybdate, cerate, or permanganate or a rare-earth salt has been used in phosphating baths to improve the corrosion protection of phosphate conversion coatings on magnesium alloys [17-20], but there are few published reports on the effects of chelating agents on the electrochemical behavior, microstructure, composition, and corrosion protection of these coatings.

In this paper, three chelating agents—tetrasodium pyrophosphate (TSPP), amino trimethylene phosphonic acid (ATMP), and ethylene diamine tetraacetic acid (EDTA)—were added into the basic phosphating bath containing ZnO, H<sub>3</sub>PO<sub>4</sub>, NaF, C<sub>4</sub>H<sub>6</sub>O<sub>6</sub>Na<sub>2</sub>, and NaNO<sub>3</sub>, respectively. The phosphate conversion coatings were formed on the magnesium alloy AZ91D derived from various phosphating baths, each containing one of the following chelating agents in the basic phosphating bath: TSPP, ATMP, and EDTA. For comparison, the phosphate conversion coating also was formed on the magnesium alloy AZ91D derived from the basic phosphating bath, which didn't contain any chelating agents. The electrochemical behavior, microstructure, composition, and corrosion protection of the phosphate conversion coatings were investigated by using potentiodynamic polarization (PDP) curves, electrochemical impedance spectroscopy (EIS) plots, scanning electron microscopy (SEM) observations, X-ray diffraction (XRD) analyses, X-ray photoelectron spectroscopy (XPS) analyses, and salt-water immersion (SWI) tests.

## 2. EXPERIMENTAL

### 2.1 Materials and preparation

The material was the AZ91D die-casting magnesium alloy with the chemical composition (wt %): Al, 9.4; Zn, 0.82; Mn, 0.23; Si, 0.01; Cu, 0.02; Ni 0.0021; Fe, 0.005. Samples were prepared by cutting the magnesium alloy AZ91D to many small plates with the dimensions of 25mm×15mm×5mm.

## 2.2 Preparation of the phosphate conversion coatings on the magnesium alloy AZ91D

Samples were manually finished up to 1000 grit SiC abrasive papers, and rinsed with de-ionized water and degreased in alcohol. The phosphate conversion coatings were formed on the surface of the samples at 45 °C for 20 min by immersing the samples into the phosphating baths with the compositions as shown in Table 1, and the chemical formulas and molecular structures of the three chelating agents were shown in Fig.1.

**Table 1.** The compositions of the phosphating baths.

Bath	compositions (g/L)
Basic bath	ZnO, 2.0; H <sub>3</sub> PO <sub>4</sub> , 12.0; NaF, 1.0; C <sub>4</sub> H <sub>6</sub> O <sub>6</sub> Na <sub>2</sub> , 4.0; NaNO <sub>3</sub> , 6.0.
TSPP bath	Basic bath +TSPP, 0.5
ATMP bath	Basic bath +ATMP, 0.5
EDTA bath	Basic bath +EDTA, 0.5

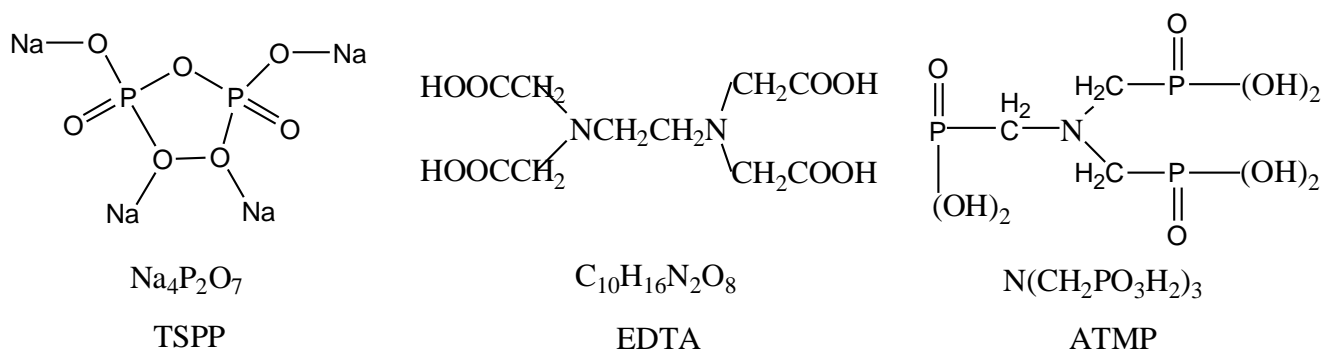


**Figure 1.** The chemical formulas and molecular structures of the three chelating agents

## 2.3 Electrochemical measurements

The electrochemical measurements were carried out in 3.5 % NaCl aqueous solution, which was prepared by analytical grade reagent and de-ionized water. The phosphate conversion coatings were coated with epoxy resin, leaving a work area of 1.0 cm<sup>2</sup> as the working electrode exposed to 3.5 % NaCl aqueous solution. The potentiodynamic polarization (PDP) curves were measured by a CS300 system (China), and the potential scanning rate was 0.5 mV/s. The EIS plots were measured by a Princeton PAPST2273 instrument (USA). The amplitude of the EIS perturbation signal was 10 mV, and the frequency range was from 10<sup>5</sup> to 10<sup>-2</sup> Hz.

A typical three electrode system was used for all the electrochemical measurements. The three electrode system was composed of the saturated calomel electrode (SCE) as reference, the platinum sheet as counter, and the working electrode. All electrochemical measurements were measured in a container under the temperature (25±3 °C) and the pH (7±0.5) controlled by a digital pH meter and a thermostatic water bath.

#### 2.4 Scanning electron microscopy (SEM) observations

The microstructure of the phosphate conversion coatings was observed by a SEM (USA), and the energy used for analyses was 20 kV.

#### 2.5 X-ray diffraction (XRD) and X-ray photoelectron spectroscopy (XPS) analyses

The phase composition and element composition of the phosphate conversion coatings were determined by a XRD (Japan) and a XPS (USA), respectively.

#### 2.6 Salt-water immersion (SWI) tests

The magnesium alloy AZ91D samples coated with the phosphate conversion coatings were immersed into 3.5% NaCl aqueous solution, and the corrosion condition on the surface of the magnesium alloy AZ91D samples were recorded by a digital camera. During SWI test, the pH and the temperature of 3.5% NaCl aqueous solution were kept in a constant state by a digital pH meter and a thermostatic water bath too.

### 3. RESULTS AND DISCUSSION

#### 3.1 Electrochemical behavior

##### 3.1.1 PDP curves

Fig.2 shows the PDP curves of the phosphate conversion coatings formed on the magnesium alloy AZ91D derived from TSPP bath, ATMP bath, EDTA Bath, and Basic Bath. The cathode sections of the PDP curves corresponded to the evolution of the hydrogen, and the anodic sections of the PDP curves was very important to reflect the corrosion protection of the phosphate conversion coatings. With the increase of anodic over-voltage, polarization current density ( $i$ ) increases through the whole range of the anodic sections of the PDP curves. The phosphate conversion coatings derived from TSPP bath and ATMP have more positive corrosion potential ( $E_{\text{corr}}$ ) and lower corrosion current density ( $i_{\text{corr}}$ ) than those derived from Basic bath and EDTA Bath do, and the  $E_{\text{corr}}$  and  $i_{\text{corr}}$  of the phosphate conversion coating derived from EDTA bath is invariable compared with those of the phosphate conversion coating derived from Basic Bath. The  $E_{\text{corr}}$  of the phosphate conversion coatings shift positively in the order: TSPP>ATMP>EDTA. The  $i_{\text{corr}}$  of the phosphate conversion coatings decrease in the order: TSPP>ATMP>EDTA.  $E_{\text{corr}}$ ,  $i_{\text{corr}}$ , and anodic/cathodic Tafel slope ( $\beta_A$  and  $\beta_K$ ) obtained from the PDP curves are showed in Table 2. According to the approximately linear polarization behavior near OCP, the polarization resistance ( $R_p$ ) of the phosphate conversion coatings was calculated by Stern-Geary equation [21].

From the results in Fig.2 and table 2, the corrosion protection of the phosphate conversion coating derived from TSPP bath is better than that of the phosphate conversion coatings derived from ATMP bath, EDTA Bath, and Basic bath because the phosphate conversion coating derived from TSPP bath has more positive  $E_{corr}$  and lower  $i_{corr}$  than the phosphate conversion coatings derived from ATMP bath, EDTA Bath, and Basic bath do.

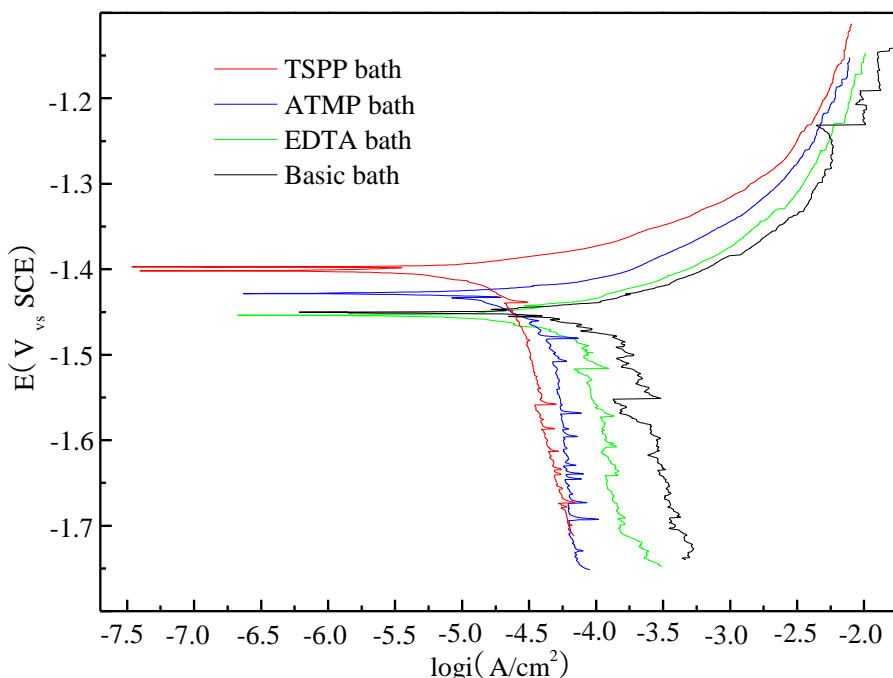


**Figure 2.** PDP curves of the phosphate conversion coatings derived from TSPP bath, ATMP bath, EDTA Bath, and Basic Bath in 3.5% NaCl aqueous solution.

**Table 2.** Parameters of PDP curves of the phosphate conversion coatings derived from TSPP bath, ATMP bath, EDTA Bath, and Basic Bath in 3.5% NaCl aqueous solution.

Bath	$E_{corr}$ (V vs SCE)	$i_{corr}$ (A/cm <sup>2</sup> )	$\beta_A$ (mV/dec.)	$\beta_K$ (mV/dec.)	$R_p$ ( $\Omega$ )
TSPP	-1.40	$0.85 \times 10^{-5}$	71.53	73.84	$2.16 \times 10^4$
ATMP	-1.43	$1.01 \times 10^{-5}$	75.86	72.49	$1.87 \times 10^4$
EDTA	-1.45	$2.80 \times 10^{-5}$	84.62	64.27	$8.76 \times 10^3$
Basic	-1.45	$3.00 \times 10^{-5}$	85.13	65.75	$8.52 \times 10^3$

### 3.1.2 EIS plots

Fig.3 shows the EIS plots of the phosphate conversion coatings derived from TSPP bath, ATMP bath, EDTA Bath, and Basic Bath. From the Nyquist plots, all of the phosphate conversion coatings show two capacitive loops, one for high and intermediate frequency and another depressed capacitive loop for low frequency. It was reported in literatures that the high frequency capacitive loop

corresponded to the charge transfer and film effect [22-24], and the low frequency capacitive loop corresponded to the presence of a protective film, the phosphate conversion coatings here. While, all of the phosphate conversion coatings show no evidence of an inductive loop, and no inductive loop suggests that the magnesium alloy AZ91D samples did not undergo localized corrosion during EIS measurements. The radius of the capacitive loop of the phosphate conversion coating derived from TSPP bath is larger than that of the phosphate conversion coatings derived from ATMP bath, EDTA bath, and Basic bath. From the Bode plots, the  $Z_{0.01\text{Hz}}$  of the phosphate conversion coating derived from TSPP bath is about  $4.0 \times 10^4 \Omega \cdot \text{cm}^2$ , and this value of the phosphate conversion coatings derived from ATMP bath, EDTA bath, and Basic Bath are  $2.0 \times 10^4 \Omega \cdot \text{cm}^2$ ,  $1.0 \times 10^4 \Omega \cdot \text{cm}^2$ , and  $1.0 \times 10^4 \Omega \cdot \text{cm}^2$ , respectively.

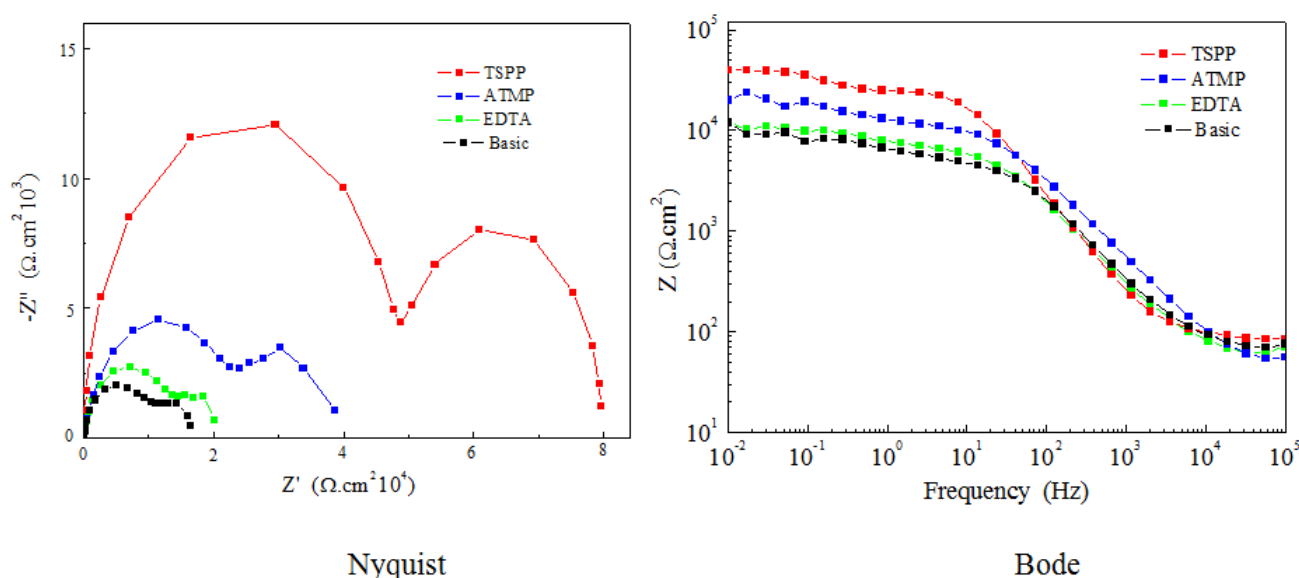


**Figure 3.** EIS plots of the phosphate conversion coatings derived from TSPP bath, ATMP bath, EDTA Bath, and Basic Bath in 3.5% NaCl aqueous solution.

In order to further clarify the electrochemical behavior, the analyses of electrical equivalent circuit for EIS plots were applied. According to the results of Fig.3 and the interface character between the phosphate conversion coatings and 3.5% NaCl aqueous solution, the EIS of the phosphate conversion coatings in 3.5% NaCl aqueous solution were interpreted by the electrical equivalent circuit as described in Fig.4. In Fig.4,  $R_s$ ,  $C_c$ ,  $R_c$ ,  $C_d$ , and  $R_t$  represent solution resistance, capacitance and resistance of the phosphate conversion coatings, capacitance of the double layer, and charge transfer resistance of interface between the phosphate conversion coatings and 3.5% NaCl aqueous solution, respectively. The value of the circuit elements are calculated by the ZSIMPWIN software and showed in Table 3. From Table 3, the maximum of  $R_c$  and  $R_t$  and the minimum of  $C_d$  are obtained from the phosphate conversion coating derived from TSPP bath. Because the  $C_d$  was related to the actual corrosion area, it was concluded from the  $C_d$  that the corrosion area of the phosphate conversion coating derived from TSPP bath was less than that of the phosphate conversion coatings derived from

ATMP bath, EDTA bath, and Basic bath, namely, the phosphate conversion coating derived from TSPP bath provided better corrosion protection for the magnesium alloy AZ91D than the phosphate conversion coatings derived from ATMP bath, EDTA bath, and Basic bath did. The better corrosion protection of the phosphate conversion coating derived from TSPP bath also could be confirmed by  $R_c$  and  $R_t$  because this two parameters were related to the insulativity of phosphate conversion coatings. From Table 3, the phosphate conversion coating derived from TSPP bath has much higher  $R_c$  and  $R_t$  than the phosphate conversion coatings derived from ATMP bath, EDTA bath, and Basic bath does.

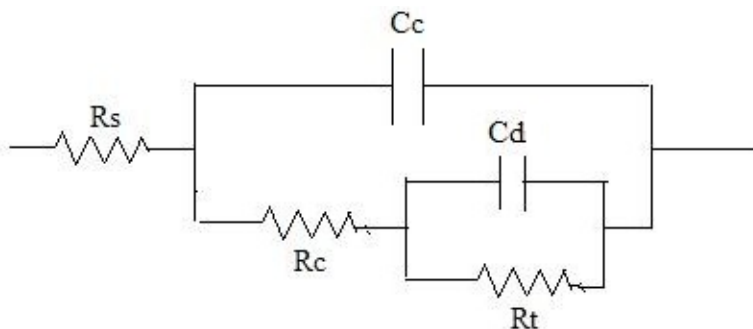


**Figure 4.** The electrical equivalent circuit to interpret the electrochemical behavior

**Table 3.** Parameters of EIS plots of the phosphate conversion coatings derived from TSPP bath, ATMP bath, EDTA Bath, and Basic Bath in 3.5% NaCl aqueous solution.

Bath	Chelating agent	$C_c$ (F/cm <sup>2</sup> )	$R_c$ (Ω·cm <sup>2</sup> )	$C_d$ (F/cm <sup>2</sup> )	$R_t$ (Ω·cm <sup>2</sup> )
TSPP	TSPP	$6.65 \times 10^{-6}$	$2.46 \times 10^3$	$7.92 \times 10^{-4}$	$1.53 \times 10^3$
ATMP	ATMP	$1.47 \times 10^{-5}$	$1.40 \times 10^3$	$1.06 \times 10^{-3}$	$8.65 \times 10^2$
EDTA	EDTA	$7.53 \times 10^{-5}$	$5.55 \times 10^2$	$8.47 \times 10^{-3}$	$4.58 \times 10^2$
Basic	None	$7.92 \times 10^{-5}$	$4.48 \times 10^2$	$9.03 \times 10^{-3}$	$4.39 \times 10^2$

All above results from PDP curves and EIS plots showed that the phosphate conversion coating derived from TSPP bath provided better corrosion protection for the magnesium alloy AZ91D than the phosphate conversion coatings derived from ATMP bath, EDTA bath, and Basic bath did. The effectiveness of the three chelating agents was in the order: TSPP>ATMP>EDTA.

### 3.2 SEM observations

In order to explain the results from electrochemical measurements, the microstructure of the phosphate conversion coatings were observed by SEM, as showed in Fig.5. From Fig.5 (a) and Fig.5 (c), the phosphate conversion coatings derived from EDTA bath and Basic bath have many big crystal clusters, and there are many smaller crystal clusters between the big crystal clusters. This microstructure destroyed the electrochemical uniformity of the phosphate conversion coatings when the coatings touched with electrolyte solution (3.5% NaCl aqueous solution).The corrosive Cl<sup>-</sup> ions in

3.5% NaCl aqueous solution could induce the corrosion of the magnesium alloy AZ91D through the gaps between big crystal clusters and smaller crystal clusters. The similar SEM morphology of the phosphate conversion coating has been observed by other authors [17], and it has been confirmed that the protection property of small crystal clusters is better than that of big crystal clusters for magnesium alloy substrate.

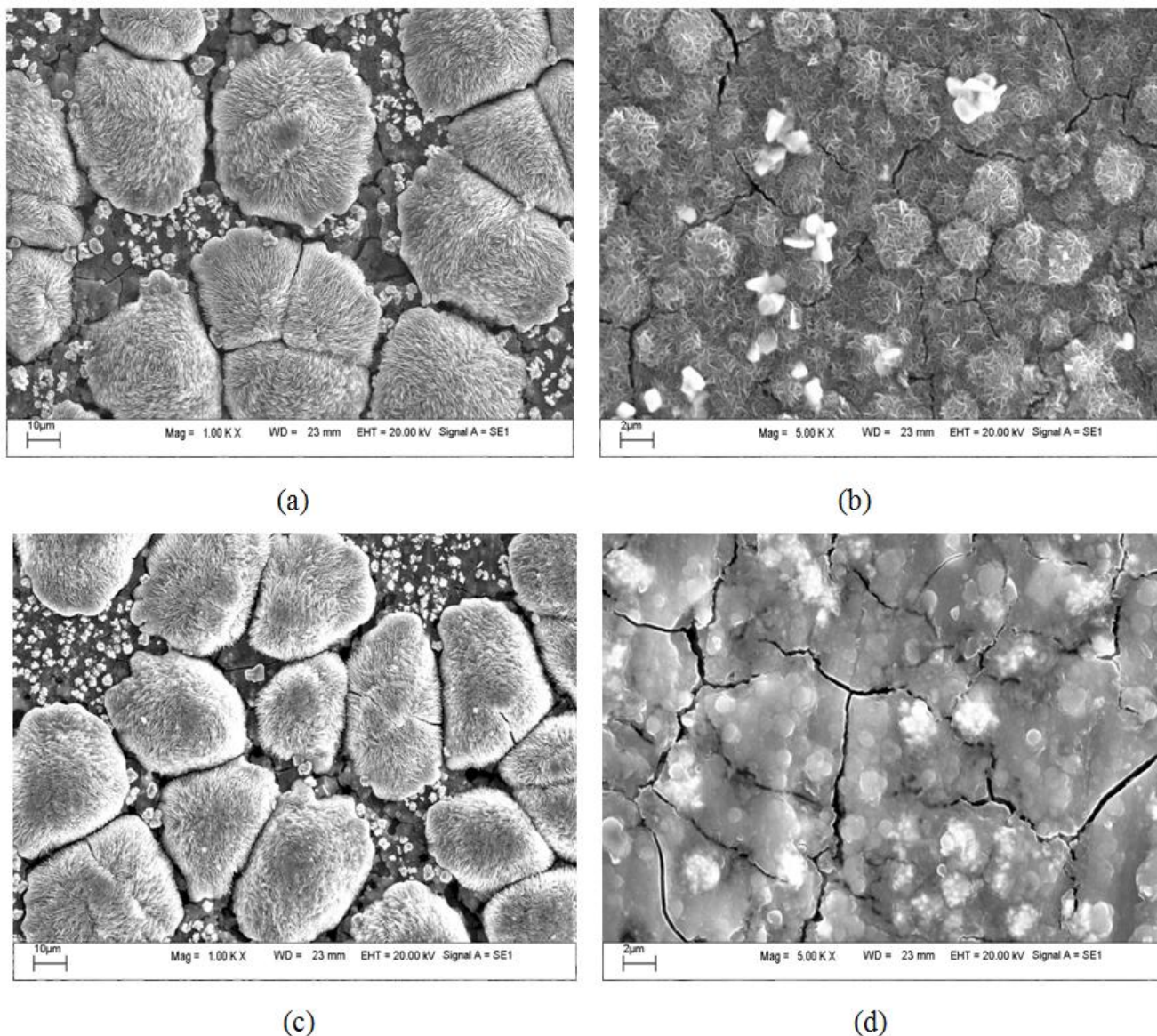


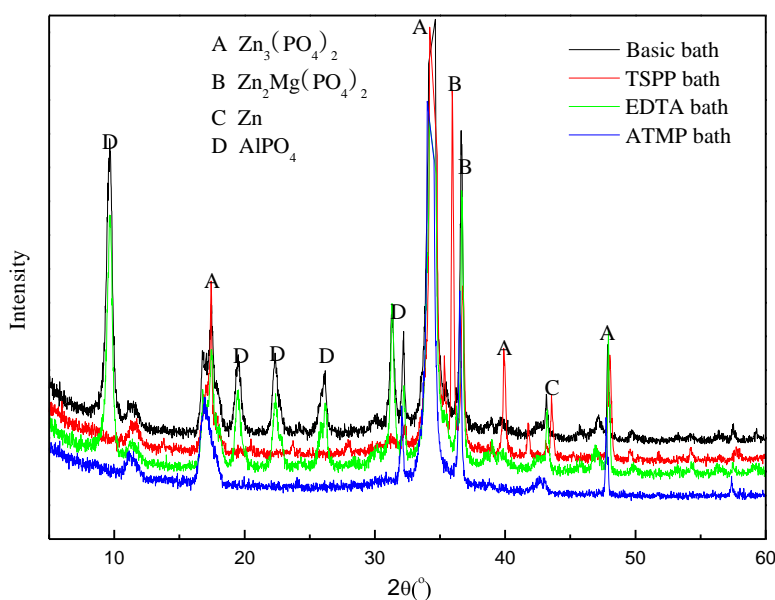
**Figure 5.** SEM of the phosphate conversion coatings derived from (a) Basic bath, (b) TSPP bath, (c) EDTA Bath, and (d) ATMP Bath.

From Fig.5 (b) and Fig.5 (d), the phosphate conversion coatings derived from TSPP bath and ATMP bath are more uniform and compact than those derived from EDTA bath and Basic bath. However, there are some cracks on the phosphate conversion coatings derived from TSPP bath and ATMP bath because of the hydrogen evolution reaction. The number and total area of cracks on the phosphate conversion coating derived from TSPP bath is less than that of cracks on the phosphate

conversion coating derived from ATMP bath; therefore, the corrosion protection of the phosphate conversion coating derived from TSPP bath was better than that of the phosphate conversion coating derived from ATMP bath. So adding TSPP refined the microstructure of the crystal clusters, and the phosphate conversion coating derived from TSPP bath, with the most uniform, compact, and integral crystal clusters, provided better corrosion protection for the magnesium alloy AZ91D. This result is consistent with the investigations from Niu et.al [8,10,18] and Kouisni et.al [19, 20]: the phosphate conversion coatings which have smaller crystal clusters and compact structure can provide better protection property.

### 3.3 XRD and XPS analyses

Fig.6 shows the XRD patterns of the phosphate conversion coatings derived from TSPP bath, ATMP bath, EDTA bath, and Basic bath. It is indicated that the major phases of the phosphate conversion coatings derived from TSPP bath and ATMP bath were composed of  $Zn_3(PO_4)_2$ ,  $Zn_2Mg(PO_4)_2$  and Zn. This XRD results are consistence with the studies from Li et.al [17] and Yong et.al [18]. While, except  $Zn_3(PO_4)_2$ ,  $Zn_2Mg(PO_4)_2$ , and Zn, the extra phase of  $AlPO_4$  was detected by XRD in the phosphate conversion coatings derived from EDTA bath and Basic bath. According to previous investigations, the main phase composition of phosphate conversion coatings on magnesium alloy is  $Zn_3(PO_4)_2$ ,  $Zn_2Mg(PO_4)_2$ , and Zn, so the reason of the presence of  $AlPO_4$  needed further studies.

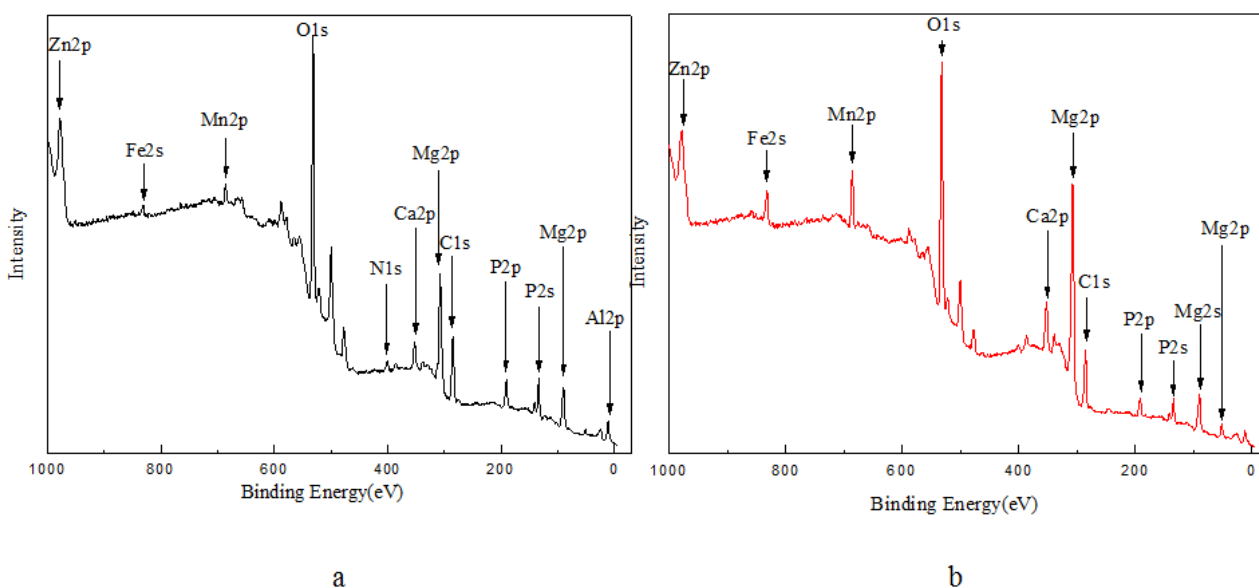
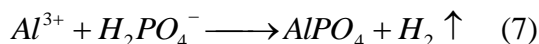
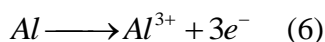
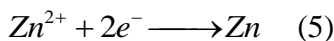
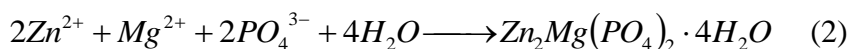
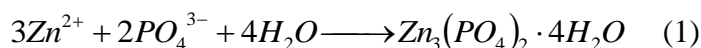


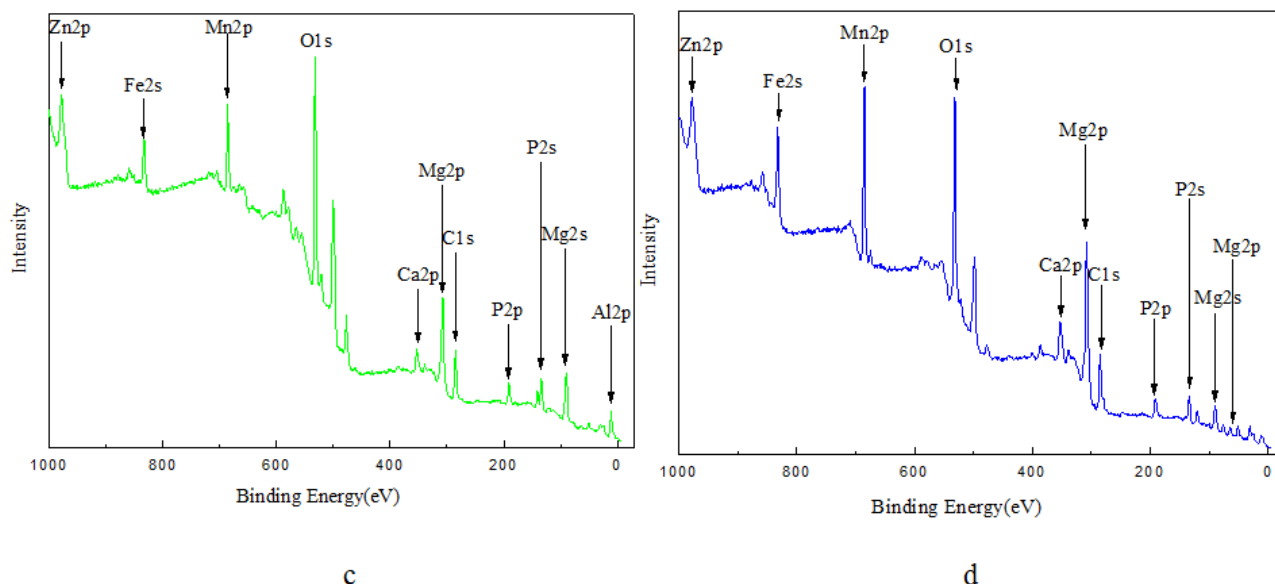
**Figure 6.** XRD patterns of the phosphate conversion coatings derived from TSPP bath, ATMP bath, EDTA Bath, and Basic Bath.

Fig.7 shows the XPS patterns of the phosphate conversion coatings derived from TSPP bath, ATMP bath, EDTA bath, and Basic bath. For the phosphate conversion coatings derived from TSPP bath and ATMP bath, Zn, O, Mg, and P were detected as the major elements. But for the phosphate conversion coatings derived from EDTA bath and Basic bath, one more major element, Al, was detected.

More detailed XPS analyses of specific electron binding energies of elements are showed in Fig.8. According to the data previous literatures [25], the XPS peaks of each element should be resulted from the corresponding compounds. Thus, it could be supposed that  $Zn_3(PO_4)_2$ ,  $Zn_2Mg(PO_4)_2$  and Zn probably constituted the phosphate conversion coatings derived from TSPP bath and ATMP bath, while  $Zn_3(PO_4)_2$ ,  $Zn_2Mg(PO_4)_2$ , Zn and  $AlPO_4$  probably constituted the phosphate conversion coatings derived from EDTA bath and Basic bath. This result was consistent with XRD analyses. The similar results of XPS have been reported by other authors [18].

From the above results of XPD and XPS, the formation mechanisms of the phosphate conversion coatings is attribute to following reactions:





**Figure 7.** XPS patterns of the phosphate conversion coatings derived from (a) Basic bath, (b) TSPP bath, (c) EDTA Bath, and (d) ATMP Bath.

### 3.4 SEI tests

Fig.9 shows the results of SWI tests of the magnesium alloy AZ91D samples coated with the phosphate conversion coatings derived from TSPP bath, ATMP bath, EDTA bath, and Basic bath. After 5 hours in SWI tests, there are many black spots or corrosion pits appear on the samples. As immersion time went on, the black spots and corrosion pits widely extended on the samples derived from EDTA bath and Basic bath. During immersion time of 20h to 80h, the old corrosion pits became bigger and deeper, and many new corrosion pits appeared on the surface. When immersion time reached 80h, the samples derived from EDTA bath and Basic bath had been corroded heavily, and the sample derives from EDTA bath was corroded lighter than that derived from Basic bath. However, for the samples derived from TSPP bath and ATMP bath, the surface was kept smooth and homogeneous relatively during the SWI tests.

From the results in Fig.9, the phosphate conversion coatings derived from EDTA bath and Basic bath had the worse corrosion protection and were wrecked only for 5-20h in 3.5% NaCl aqueous solution. From the accumulated corrosion damage of the phosphate conversion coatings derived from EDTA bath and Basic bath, the corrosive  $\text{Cl}^-$  ions had reached the AZ91D substrate, suggest that the phosphate conversion coatings derived from EDTA bath and Basic bath could only afford a transitory corrosion protection for the magnesium alloy AZ91D. However, the phosphate conversion coatings derived from TSPP bath and ATMP bath had better corrosion protection based on the results of SWI tests, and this results was consistent with SEM observation.

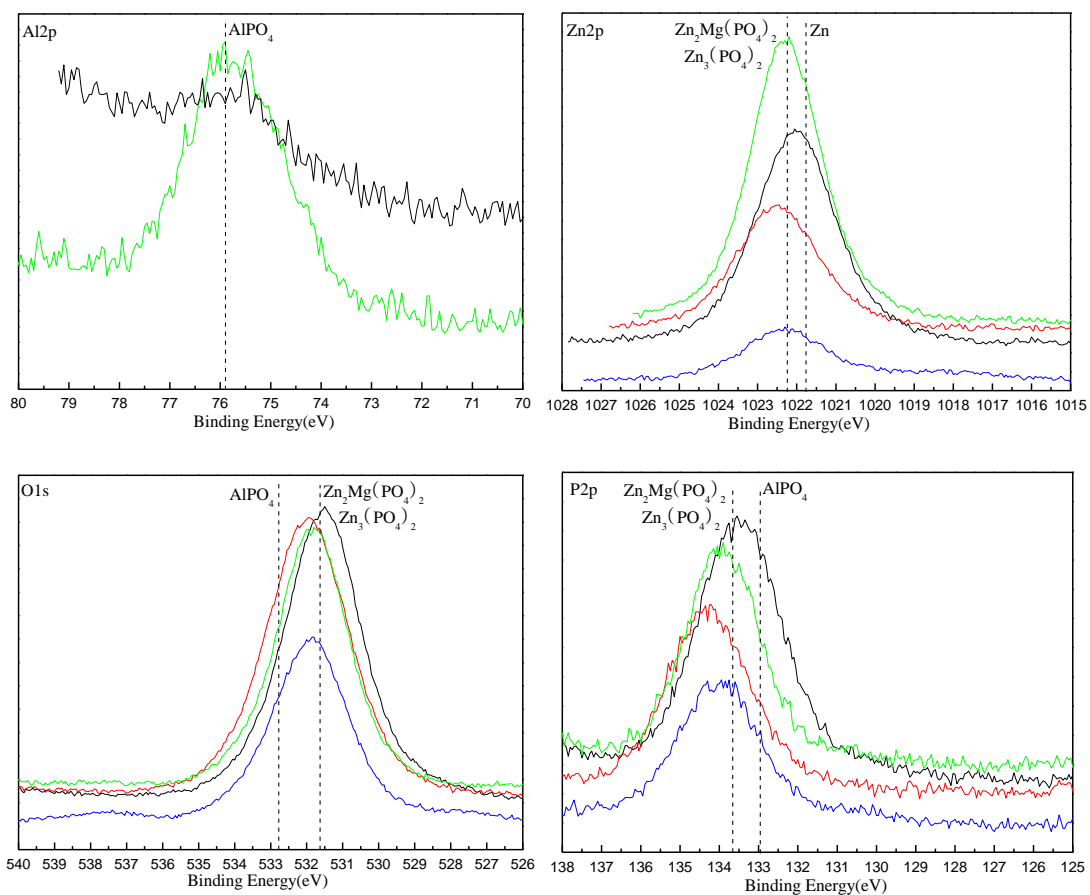


**Figure 8.** XPS intensities of Al2p, Zn2p, O1s, P2p of the phosphate conversion coatings derived from (a) Basic bath, (b) TSPP bath, (c) EDTA Bath, and (d) ATMP Bath.

Additive	0h	5h	20h	30h	50h	80h	110h
none							
TSPP							
EDTA							
ATMP							

**Figure 9.** Results of SWI tests of the magnesium alloy AZ91D samples coated with the phosphate conversion coatings derived from TSPP bath, ATMP bath, EDTA bath, and Basic bath.

#### 4. CONCLUSIONS

① TSPP was more beneficial to the corrosion protection of the phosphate conversion coating on the magnesium alloy AZ91D than ATMP and EDTA were.

② TSPP refined the microstructure of the crystal clusters, and the phosphate conversion coating derived from the phosphating bath containing TSPP had the most uniform, compact, and integral crystal clusters and provided better corrosion protection for the magnesium alloy AZ91D.

③ XRD and XPS analyses indicated that the phosphate conversion coatings mainly were composed of  $Zn_3(PO_4)_2$ ,  $Zn_2Mg(PO_4)_2$  and Zn.

#### References

1. G.L.Song and D.StJogn, *Corrosion Science*, 46 (2004) 1381.
2. J.E.Gray and B. Luan, *Journal of Alloys and Compounds*, 336 (2002) 88.
3. G.L.Song and D.H.StJohn, *Material and Corrosion*, 56 (2005) 15.
4. T.S.Shih, J.B.Liu and P.S.Wei, *Materials Chemistry and Physics*, 104 (2007) 497.
5. A.Bakkar and V.Neubert, *Electrochemistry Communication*, 9 (2007) 2428.
6. X.B.Tian, C.B.Wei, S.Q.Yang, Ricky K.Y.Fu and Pual K.Chu, *Surface & Coating Technology*, 198 (2005) 454.
7. C.G.da Silva, A.N.Correia, P.de Lima-Neto, I.C.P. Margarit and O.R.Mattos, *Corrosion Science*, 47 (2005) 709.
8. L.Y.Niu, Z.H.Jiang, G.Y.Li, C.D.Gu and J.S.Lian, *Surface & Coatings Technology*, 200 (2006) 3021.
9. R.G.Duarte, A.C.Bastos, A.S.Castela and M.G.S.Ferreira, *Progress in Organic Coatings*, 52 (2005) 320.
10. G.Y.Li, L.Y.Niu, J.S.Lian and Z.H.Jiang, *Surface & Coatings Technology*, 176 (2004) 215.
11. X.Sun, D.Susac, R.Li, K.C.Wong, T.Foster and K.A.R.Mitchell, *Surface & Coatings Technology*, 155 (2002) 46.
12. D.Zimmermann, A.G.Munoz and J.W.Schultze, *Electrochimica Acta*, 48 (2003) 3267.
13. K.Z.Chong and T.S.Shih, *Materials Chemistry and Physics*, 80 (2003) 191.
14. L.Lazzarotto, C.Marechal, L.Dubar, A.Dubois and J.Oudin, *Surface & Coatings Technology*, 122 (1999) 94.
15. R.C.Zeng, Z.D.Lan, L.H.Kong, Y.D.Huang and H.Z.Cui, *Surface & Coatings Technology*, 205 (2011) 3347.
16. W.Q.Zhou, D.Y.Shan, E.H.Han and W.Ke, *Corrosion Science*, 50 (2008) 329.
17. Q.Li, S.Q.Xu, J.Y.Hu, S.Y.Zhang, X.K.Zhong and X.K.Yang, *Electrochimica Acta*, 55 (2010) 887.
18. Z.Y.Yong, J.Zhu, C.Qiu and Y.L.Liu, *Applied Surface Science*, 255 (2008) 1672.
19. L.Kouisni, M.Azzi, M.Zertoubi, F.Dalard and S.Maximovitch, *Surface & Coatings Technology*, 185 (2004) 58.
20. L.Kouisni, M.Azzi, F.Dalard and S.Maximovitch, *Surface & Coatings Technology*, 192 (2005) 239.
21. H.P.Duan, K.Q.Du, C.W.Yan and F.H.Wang, *Electrochimica Acta*, 51 (2006) 2898.
22. R.Walter and M.B.Kannan, *Materials & Design*, 32 (2011) 2350.
23. F.Zucchi, V.Grassi and A.Frignani, *Journal of Applied Electrochemistry*, 36 (2006) 195.
24. L.F.Guo, T.M.Yue and H.C.Man, *Journal of Materials Science Letter*, 40 (2005) 531.

25. C.D.Wagner and D.E.Bicjham, NIST X-ray photoelectron spectroscopy database NIST, (1989).
26. R.Amini and A.A.Sarabi, *Applied Surface Science*, 257 (2011) 7134.

© 2014 The Authors. Published by ESG ([www.electrochemsci.org](http://www.electrochemsci.org)). This article is an open access article distributed under the terms and conditions of the Creative Commons Attribution license (<http://creativecommons.org/licenses/by/4.0/>).